**Atmospheric
Chemistry
and Physics
Discussions**

Tracer diffusion

P. S. Anderson

Title Page

Abstract	Introduction
Conclusions	References
Tables	Figures

◀ | ▶|

◀ | ▶

Back | Close

Full Screen / Esc

Printer-friendly Version

Interactive Discussion

EGU

Behaviour of tracer diffusion in simple atmospheric boundary layer models

P. S. Anderson

British Antarctic Survey, Madingley Road, Cambridge, CB3 0ET, UK

Correspondence to: P. S. Anderson (philip.s.anderson@bas.ac.uk)

Abstract

1-D profiles and time series from an idealised atmospheric boundary layer model are presented, which show agreement with measurements of polar photogenic NO and NO_2. Diffusion models are increasingly being used as the framework for studying tropospheric air chemistry dynamics. Models based on standard boundary layer diffusivity profiles have an intrinsic behaviour that is not necessarily intuitive, due to the variation of turbulent diffusivity with height. The relatively simple model provides both a programming and a conceptual tool in the analysis of observed trace gas evolution. A time scale inherent in the model can be tuned by fitting model time series to observations. This scale is then applicable to the more physically simple but chemically complex zeroth order or box models of chemical interactions.

1 Introduction

Recent polar air chemistry field campaigns have highlighted the need to integrate air chemistry, boundary layer physics, snow chemistry and snow physics in order to understand the behaviour of trace gas evolution in the lower troposphere. The large investment required to equip a site with both micro-meteorological equipment and a suitable air chemistry facility confines most contemporary studies to existing static research stations, such as (from south to north), South Pole, Dome C, Halley, Greenland Summit, Barrow and Alert (Davis et al., 2004; Jones et al., 2006[1]; Dibb and Jaffrezo, 1997). Inter-site comparisons and contrasts can be made, given the differences in latitude, altitude and maritime influences. King et al. (2006) note that Halley and Dome C experience similar top of the atmosphere solar forcing due to their latitudinal similarities yet they still experience significantly different climatologies due to altitude differences.

---

[1]Jones, A. E., Wolff, E. W., Salmon, R. A., and Bauguitte, S. J.-B.: An Overview of the CHABLIS Campaign, Atmos. Chem. Phys. Discuss., in preparation, 2006

Title Page

Abstract	Introduction
Conclusions	References
Tables	Figures

◄◄ ►►

◄ ►

Back Close

Full Screen / Esc

Printer-friendly Version

Interactive Discussion

EGU

Inter-site climatological difference must be taken into account when assessing the difference in the chemical behaviour of the atmosphere.

The physical dynamics of a system can occasionally be the cause of rapidly varying or extremes in chemical signature in the environment (Jones et al., 2006). Frontal events bring air masses with differing histories to the sample inlet, and the frontal interface may be remarkably narrow. Identifying when an observed tracer variation is due to chemical dynamics or due to physical advection requires either spatial measurements or a reliable boundary layer model of the atmosphere. In polar studies, cost often preclude such luxuries as the former. The onus is therefore on the intuitive skill of the researcher to tease out the truth from the message, and for polar environmental studies, these skills need to be multidisciplinary.

When a perfect model of a system is unavailable, conceptual models become increasingly vital to assist our interpretation of experimental data. Conceptual models are useful in any scientific endeavour, and the exchange of such concepts between different schools often generate their own insights. For the polar boundary layer physics and chemistry community, the interchange of ideas is proving increasingly fruitful. The behaviour of the idealised boundary layer diffusion scheme is both simple enough to envisage, whilst affording some level of accuracy, especially during the polar summer when the atmosphere is relatively well mixed. The model is likely to be unsuitable for studying trace gas transfer within the very stable boundary layer, however, due to significant complexities that are not captured by the simple diffusive scheme (Mahrt, 1998).

Direct experience of diffusion is limited to approximately linear systems, such as the flow of heat through a conductor or the percolation of cooking smells through the house. In an exact linear diffusive system the resulting flux is directly proportional to a gradient, with the diffusivity being the constant of proportionality. In contrast, the classical atmospheric boundary layer diffusive model incorporates a variable diffusivity, one that is proportional to the height above the surface. When used in 1-D models, this form of diffusivity generates profiles that evolve towards straight lines when plotted

Tracer diffusion

P. S. Anderson

Printer-friendly Version

Interactive Discussion

EGU

against ln(z) and are known as log-linear profiles.

With a diffusivity linearly proportional to height, there is an implied zero diffusivity at the surface; this is evidently an unrealistic representation because we know that moisture and other trace gases can diffuse across the surface boundary. Some compromise in the model is required very close to the surface which is achieved with a finite roughness length, z_0, This length scale is defined as the height at which the log-linear profile extrapolates to zero. Over typical snow surfaces, the roughness length for momentum, z_0, can be as small as 50 micron (King and Anderson, 1994) and other roughness lengths (e.g. for heat or trace gas diffusion) are assumed to be of a similar scale. A diffusivity that scales with z will necessarily become very small at the roughness length, and require very large gradients to maintain a flux.

In both the real world and 1-D diffusion models there is usually some upper level where the diffusivity becomes zero. This level defines the top of the boundary layer, and may be regarded as the upper extent of a containment vessel for surface processes. Intuition would indicate that the depth of the boundary layer and the rate of exchange between the surface and the rest of the atmosphere would be the main factors governing the shape of the resulting profiles. This detracts from two other significant factors; the variation of diffusivity with height, and the loss of the tracer out of the system. As will be shown below, for certain cases, the depth of the boundary layer is irrelevant in determining the trace gas profile or the time series near the surface.

The model used to generate the profiles presented here is the simplest physical description that represents a real atmospheric boundary layer. The modelled concentration of a virtual tracer in the near surface layer agree well with real measurements made at the Halley research station in Antarctica. The model is relatively insensitive to physical parameters such as wind speed or boundary layer depth, compared to the sensitivity to changes in typical values of the tracer decay (or loss) term, τ. The loss term can be tuned to real time series, and hence provides the effective time scale that is relevant for zeroth order box models of realistically complex chemistry.

The model equations and boundary conditions are described in the first part of the

|◄ | ►|
◄ | ►

Back | Close

Full Screen / Esc

Printer-friendly Version

Interactive Discussion

EGU

Methods section; certain practical aspects of solving the equations are discussed, e.g. using a logarithmic grid spacing. This is followed by the averaging and function fitting techniques used to analyse the NO and NO_2 field data, ready for comparison to model generated time series.

5   The Results section presents typical profiles and time series of tracer concentration that are solutions to the diffusion equation, and the effects of modifying physical parameters such as boundary layer depth, and roughness length.

The Discussion section describes the time scales for which the boundary layer depth is not important, and some consequences of log-linear profiles. The Discussion ends

10   with possible explanations for asymmetry in the observed NO_x data time series.

2   Method

2.1   Model description

The model is a one-dimensional time-dependent diffusion scheme with variable diffusivity, K. The diffusivity is linearly proportional to height, z, according to surface layer

15   similarity theory. There is no flux across the upper boundary, that is, the gradient is forced to be zero. The height of this upper level, h, is prescribed and defines the top of the turbulent boundary layer. The lower boundary condition assumes a flux of trace gas which is proportional to the actinic surface flux, $J(t)$:

$$K \frac{dC}{dz}\bigg|_{z=z0} \propto J(t) \tag{1}$$

20   where C is the concentration. Actual $J(t)$ at the site is unknown, so a proxy is taken from the estimated downwelling shortwave radiation at the surface. Surface radiation is assumed to be proportional to the top of atmosphere solar flux, and hence atmospheric absorption is neglected. J is a function of time of year and latitude, and varies diurnally. The model is given a certain date which then defines $J(t)$ for a 24-h period

Tracer diffusion

P. S. Anderson

◀◀ | ▶▶

◀ | ▶

Back | Close

Full Screen / Esc

and hence the diurnal surface boundary conditions. In the model presented here, the photo-generation of tracer at the surface is taken as equal to $J(t)$, hence C is in arbitrary units per m^3. Conversion to typical real units, such as pptv, requires a conversion efficiency. Conversely, the conversion efficiency from Wm^{-2} of shortwave irradance to pptv per second of tracer may be estimated once the model has been tuned to a time series of actual data.

The diffusion model and loss term are described by

$$\frac{dC}{dt} = \frac{d}{dz}\left(K\frac{dC}{dz}\right) - \frac{C}{\tau} \tag{2}$$

where t is time, z is height, K the local diffusivity and τ a loss term which defines the rate of decay of C in a gradient-free environment. A Crank-Nicholson scheme with N levels is used to solve the difference form of Eq. (2), the levels are spaced logarithmically such that the height, z_n, of level n ($n=0{:}N-1$) is given by:

$$z_n = z_0 e^{n.\Delta z}$$
$$\Delta z = \frac{\ln(h) - \ln(z_0)}{50} \tag{3}$$

where h is the prescribed height of the upper level. For these studies the profile and time series results did not vary for N above ~50. The model time step was 5 min.

The diffusivity, $K(z)$ is given by

$$K(z) = 0.4 z u_* \tag{4}$$

where the friction velocity, u_*, is derived from the near surface form of the neutral boundary layer equation, that is:

$$\frac{0.4U}{u_*} = \ln\left(\frac{z}{z_0}\right) \tag{5}$$

where U is the wind speed at height z. The value 0.4 is the von Karman constant, usually represented by κ, the Greek letter kappa. I have used 0.4 in equations to avoid confusion with the diffusivity terms, such as K.

Tracer diffusion

P. S. Anderson

EGU

K is dependent upon z, whereas u_* is a constant. This leads to $K=0$ at the surface, which is obviously not realistic. The model assumes that this form of K is only valid for $z \geq z_0$, in accord with physical models of surface layer stress and heat flux.

In the real neutral boundary layer, u_* decreases with height in the upper boundary layer, but in the model has been kept constant throughout the domain.

To ensure stability in the model, the vertical spacing in z was logarithmic, with small spacing near the surface. The model was insensitive to level number, n, for $n>50$, and n was set to 50 throughout the analysis. The equations were solved using a standard Crank-Nicholson scheme for the diffusion time step, and then the loss term was subtracted from the resulting profile at each time step. The model was initialised with zero concentration at all levels, and then spun up for five days before the profile or time series were extracted. The model was run for $J(t)$ equivalent to 76° South in late January, in order to be comparable to the period and position of the NO and NO_2 data.

2.2 Model sensitivity

The model generates a time series of concentration profiles, $C(t,z)$ from which profiles at a given time or a time series at a given height can be extracted. The significant prognostic physical parameters in the model were domain boundaries, h and z_0 , and the wind speed, U, from which u_* and hence $K(z)$ were derived. A measure of the general behaviour of the model is given by the time lag, Δt, between maximum $J(t)$ and maximum $C(z,t)$ at a given height. Δt can then be presented graphically as a function of the loss time constant, τ. The sensitivity of the model to changes in h, z_0 and U is then shown as effects on behaviour of $\Delta t(\tau)$.

2.3 NO, NO_2 and NO_x measurements

Near surface measurements of NO and NO_2 from an Antarctic station were available as part of the CHABLIS air chemistry campaign (REF This issue: to be supplied by Anna Jones). The measurements were made in the Clean Air Sector Laboratory (CASLab)

Tracer diffusion

P. S. Anderson

EGU

at Halley, situated at 76° S 26° W on the Brunt Ice Shelf. A description of the relevant instrumentation and site layout is given in (REF This issue: to be supplied by Anna Jones). The post processing and quality control of the NO/NO$_2$ data are described in (REF This issue: to be supplied by Stephane Bauguitte). Halley's Clean Air Sec-
5 tor is equipped with a suite of micro-meteorological instruments, from which realistic estimates of the model's prognostic physical parameters have been taken.

Two case study periods of NO and NO$_2$ time series were chosen from the full data set (Fig. 1), both four days in length but differing in the amount of cloud cover. The days from the 12 to the 15 January 2005 are mostly cloud free, whilst from 20 to 23 January
10 are cloudy.

The daily NO and NO$_2$ data have a significant level of noise, confounding attempts to make direct comparisons with either the meteorology or the model output. To reduce the effect of noise, the NO and NO$_2$ data are added to give NO$_x$. Figure 2 shows the results of such binning for the two chosen case studies, using 48 bins of width 30 min,
15 error bars indicating one standard deviation. Overlaid are the bin averages in black and two fitted harmonic functions. The green curvemeteorology or the model output. To reduce the effect of noise, the NO and NO$_2$ data are added to, $A_G(t)$ is given by:

$$A_G(t) = a_0 + a_s \sin\left(2\pi t/24\right) + a_c \cos\left(2\pi t/24\right) \tag{6}$$

where time is given in hours. For the sunny data (LHS panel, Fig. 2), there is a sys-
20 tematic disagreement between the data and the harmonic function; the data are not symmetrical about the maximum. To highlight this, $A_R(t)$ was fitted, shown in red, which included both first and second harmonics, that is:

$$A_R(t) = a_0 + a_s \sin\left(2\pi t/24\right) + a_c \cos\left(2\pi t/24\right)$$
$$+b_s \sin\left(4\pi t/24\right) + b_c \cos\left(4\pi t/24\right) \tag{7}$$

The model was tuned to agree with the observed delay between maximum J at Local
25 Apparent Noon (LAN) and maximum NO$_x$ as given by a_s and a_c. Tuning was applied to the loss constant, τ, achieved by the unconstrained nonlinear minimization method

Tracer diffusion

P. S. Anderson

EGU

intrinsic to the Matlab's fminsearch function. The model output, $C(z, t)$, at $z=4$ m was taken to compare with the NO_x data; this time series is referred to as $C_4(t)$. The values of the coefficients resulting from fitting A_G and A_R to both the sunny and cloudy NO_x data of Fig. 2 are summarised in Table 1.

5　　The model output is in arbitrary units; once τ was tuned to generate the desired Δt, $C_4(t)$ was scaled to give agreement with the diurnal variation in NO_x. Hence the diurnal variance of $C_4(t)$ and NO_x are identical, but the mean of $C_4(t)$ is not necessarily the same as the mean of NO_x.

3 Results

10　3.1 Model profiles

Figure 3 shows typical profiles of $C(z, t)$ for different value of the loss constant, τ. Boundary layer depth, h, is 50 m, roughness length, z_0 is 5×10^{-5} m and wind speed, U, is 1 ms^{-1}. The left hand panels are profiles at midnight and midday for $\tau=1$ h, the right hand panels show the same profiles for a ten-fold increase in τ. The upper set of
15　panels show the profile against linear height, whereas the lower set are plotted against $\log_{10}z$. The forcing term, $J(t)$, is appropriate for late January at 76° S, and includes a few hours of darkness around midnight where $J=0$. This form of $J(t)$ was chosen to correspond to periods when NO_x data are available.

　　The upper panels demonstrate the very large gradients in $C(z, t)$ that occur at the
20　surface due to the small values of diffusivity near z_0. For the larger value of τ, (RHS) there is tracer throughout the model domain, whilst for small τ there is almost no tracer at the top. In this latter case, h could be increased indefinitely with no effect on the resulting profiles.

　　The lower panels, with a logarithmic height axis, highlight the log-linear aspect of the
25　profiles, even when the loss term is large enough for the boundary layer depth to affect $C(z, t)$.

Each panel shows the profile for midnight and midday. For small τ, almost all tracer has been lost from the domain at midnight, whilst for larger τ, the midnight values aloft exceed the midday values. Only near the surface, (z<1 m) do the midday values exceed those at midnight. The $\log_{10}$ z-axis plot (lower right) highlights this effect, with the two profiles crossing over.

3.2 Model time series

The corresponding time series of concentration at 4 m, $C_4(t)$, for the same parameters as used in the profile examples above are shown in Fig. 4. Three days are presented, showing the model has achieved a repeating cycle for the given repetitive diurnal forcing, and indicating that the spin-up time (5 days) is sufficient. The upper panel is $C_4(t)$ for τ=1 h, the lower panel for τ=10 h. The forcing term, $J(t)$, is indicated in the middle panel. When τ is large, there is residual tracer at 4 m following the dark period (t=0, 1 etc.), and hence the mean value is elevated. In both cases there is a lag observed between the maximum in J at LAN and the maximum in 4 m accumulation, but the lag is greater for larger τ .

Both traces are close approximations to 1st order harmonic functions, with only a slight asymmetry in $C_4(t)$ for τ=1 during the dark period. For model runs where the dark period is longer, this asymmetry is enhanced.

3.3 Sensitivity

In order to quantify the sensitivity of the model to changes in parameter values, two measures of the behaviour of the model are used:

- Δ_t, the time delay in the response of the tracer at 4 m $C_4(t)$ relative to the surface forcing by J.

- R, the ratio of the standard deviation of the time series to the mean value.

The broadscale behaviour of Δ_t and R as a function of the loss term, τ, can be judged from the two time series of $C_4(t)$ shown in Fig. 4. For small values of τ (upper panel) $C_4(t)$ is approximately an offset sin function with a minimum of zero and maximum that is twice the mean. The ratio, $R = \sigma C_4(t)/<C_4(t)>$ for such a function is 0.71. For large

5   values of τ (lower panel), the variability in $C_4(t)$ is smaller relative to the mean, due to the residual tracer following the night-time; hence R becomes smaller as τ increases. The delay in the peak of $C_4(t)$ from LAN increases with τ.

Δ$_t$ and R were used in the sensitivity analysis because they can be easily derived from real time series measurements, even in the presence of significant noise.

10   Figure 5 shows R and Δ_t as functions of τ for four different sets of physical parameters. $R(\tau)$ (upper panel) tends to 0.7 as τ tends to zero, decreasing for increasing τ. $\Delta_t(\tau)$ is proportional to τ for $\tau < \sim 4$ h (lower panel). For larger τ the gradient decreases, with ever larger τ only increasing the lag by a small margin. Overlaid on the figure are four model "sets". The "standard" model uses the parameters described in Table 2.

15   The other model runs use the same parameters, but with one parameter altered by a significant (but realistic) amount. These are also given in Table 2.

3.4   NO, NO$_2$ and NO$_x$ measurements

The two time series sets of NO and NO$_2$ field measurements are present in Fig. 1, along with the co-temporal surface shortwave (solar) radiation. Note that these data

20   are plotted against GMT and mean LAN is offset from GMT noon by 26 degrees, equivalent to 1 h, 44 min. The plots have not been corrected for the small additional component of the Equation of Time. Both global and diffuse radiation are shown, global being the sum of diffuse and direct shortwave radiation. On cloudy days there is no direct visible radiation (the sun is obscured) and global and diffuse measurements are

25   identical. By contrast on sunny days most shortwave is direct and the diffuse radiation is a small component of the total. An estimate of the effect of the cloud can be judged by comparing time series of these two radiation measurements.

The magnitude of the incident shortwave radiation is reduced by cloud cover, by as

EGU

much as 40% in these data, due to light being reflected from the cloud top as shown in Fig. 2. For the cloud free data (LHS panel), there is a systematic disagreement between the data and the first order harmonic function (green) indicating that the data are not symmetrical about the maximum. To emphasis this asymmetry, the second order (red) function fits far better. The difference in the maxima of the two harmonic functions is ~1 h.

In marked contrast to the sunny data, the harmonic curves on the right hand panel for the days of cloud cover are almost identical: the cloudy data are symmetrical about the maximum and there is minimal second harmonic signature in the data.

The final curve in green is $C_4(t)$, the output from the model when the loss term, τ, has been tuned to generate the same delay in peak concentration. In both cases (sunny and cloudy data), τ was tuned to match the delay given by the first order harmonic only. Note that the amplitude of the signature variance has been matched, such that the model variance equals the data variance. An alternative scaling is matching the mean values of the data and the model output. This would be just as valid given the arbitrary units of $C_4(z,t)$, and the magnitude of the scaling term is similar, but the model-to-data comparison is clearer using the variances.

There is, again, a notable difference between the two case studies. For the sunny data, the model indicates an offset relative to the harmonic fit of about 4 pptv, whereas the cloud data shows a near exact fit. The model offset observed for the sunny days is due to the larger value of τ required to match the lag maximum concentration.

4 Discussion

4.1 Steady state conditions: the log-lin profile.

Figure 3 shows profiles of tracer for two different loss time scales; τ=1 h and τ=10 h. The lower panels show the near linearity of the resulting profiles when plotted using log z. This allows a conceptual picture of the profile for different loss time scales. In

EGU

the case where $\tau=1$ h, there is very little tracer reaching the upper limit to the domain, that is, the top of the boundary layer.

For the linear profiles where τ is "sufficiently small", extrapolating the linear part of the profile to $C=0$ gives a scale height, h_C . This may be thought of as an effective trace gas boundary layer depth, analogous to the physical boundary layer depth, h. In both cases, the magnitude of a flux has decreased to zero. Multiple runs of the model with different τ and u_* indicate that:

$$h_C \propto \tau u_* \qquad (8)$$

This is not unexpected, given that τu_* is a length scale. Of interest is that the constant of proportionality is close to 0.16, that is, the square of the von Karman constant.

The τu_* scale is only applicable if $h_C<h$, which defines the term "sufficiently small" for τ. If h_C as calculated by Eq. (8) is larger than h, the depth of the boundary layer will have a significant effect on the profiles of $C(z,t)$, by capping vertical flux aloft.

An exact log-linear profile under-estimates the total mass of tracer in the column, M, by a factor of about two, due to the slight non-linearity at the upper boundary, that is, if a linear profile is fitted to $C(\ln z)$ for near surface C:

$$C_{fit}(z) = a \ln(z) + b \qquad (9)$$

then M is about twice integral of C_{fit}. The integration of Eq. (9) is

$$\int_0^{h_C} C(z)\,dz = \int_0^{h_C} a \ln(z) + b \; dz = [a.z.(\ln(z) - 1) + bz]_{z_0}^{h_C} \qquad (10)$$

Where z_0 is the roughness length, and h_C is given by $-b/a$. For the small values of z_0 observed over snow, the z_0 terms are negligible, and the function is simplifies to

$$\int_0^{h_C} C(z)\,dz = a.h_C.(\ln(h_C) - 1) + bh_C \qquad (11)$$

And hence

$$M \approx 2a.h_C.(\ln(h_C) - 1) + bh_C \qquad (12)$$

Tracer diffusion

P. S. Anderson

EGU

Knowing the total mass, M, and the extinction time scale, τ allows the surface flux, F_s, to be estimated. Under steady state conditions, or averaged over a day, the flux will be balanced by the total loss aloft, that is

$$F_s = M/\tau \tag{13}$$

The simple model provides an intuitive guide to whether boundary layer depth is a significant parameter in the dynamics of a surface flux of trace gas, and provides some useful simplifications to the expected profiles.

4.2 Asymmetry in the NO_x time series.

The two time series of NO_x measurements shown in Figs. 1 and 2 differ in a number of aspects:

– the amplitude of NO_x diurnal variability.

– the asymmetry of the same variability

– the match between the data and a simple diffusive model.

It may well be that the highly complex underlying chemistry acting to initially photo-chemically generate and then dissociate the components of NO_x is different on the two occasions; it is possible that there are differences in the history (trajectories) of the air mass at Halley during the two case studies. It may be that the different albedo, and subsequent e-folding depth of the in-snow actinic flux affects other species of trace gas which are involved in the complex air chemistry of NO_x decay (Warren, 1982). The above notwithstanding, the model can be used to investigate whether there is any simple meteorological (that is physical) explanation which fits the data.

The significant meteorological difference between the two periods was the amount of cloud cover. Shortwave radiometers confirm our personal experience that cloud cover reduces the level of insolation reaching the surface, by scattering some of the light back

Tracer diffusion

P. S. Anderson

⏮ | ⏭

◀ | ▶

Back | Close

Full Screen / Esc

Printer-friendly Version

Interactive Discussion

EGU

into space. It is hardly surprising therefore, that the magnitude of the peak in NO_x is smaller on cloudy days.

Less obvious is the effect of longwave radiation from the cloud base. Cloud cover over snow will tend to elevate the snow surface temperature until snow, cloud base
5   and intervening air are isothermal (Ambach, 1974). In polar regions, therefore, cloud free conditions may heat the surface (through enhanced insolation) or cool the surface (through reduced thermal radiation), the balance depending on a number of variables, but tending towards heating in mid-summer and cooling at other times. Surface heating can generate convection, which dramatically increases the depth of the boundary layer.
10 As an example of this effect, Fig. 6 shows a sodar plot from Halley for 30 November, 2003. Under suitable conditions, the sodar produces a time series of mixing profiles, from which can be inferred the diurnal variation in boundary layer depth, $h(t)$. Including a time dependent boundary layer depth into the model indicates that a LAN-symmetric increase then decrease in h will generate an asymmetry in measured near surface
15 concentration; not only will there be a lag in the time series as before, but the increase in concentration in the afternoon (observed at 4 m) will be slower than the decrease in early evening.

The model implementation used a modified, time dependant, diffusivity profile, $K(z,t)$, whilst maintaining the original 1-D grid; the effect on the modelled profiles
20 was therefore due to a change in diffusivity, not a compression of the boundary layer. $K(z,t)$ is derived by multiplying $K(z)$ in Eq. (4) with a 0–1 step function at the appropriate height for each time step. The step function is implemented with the convenient tanh(x) function; hence:

$$K(z,t) = 0.4.z.u_*.g(t,z)$$
$$g(t,z) = 1 - \tanh(a(z - h(t))) \tag{14}$$

25 that is, $g(t,z)$ reduces K for $z>h$. The sharpness of the cut off depends upon a, a suitable value being $a=0.2$. $h(t)$ will vary smoothly through the day and providing a time-dependent mixing depth. The sodar image of Fig. 6 shows that the actual mixed

Tracer diffusion

P. S. Anderson

[EGU](#)

layer depth can change from less than 20 m over night to over 100 m during the middle of the day; the modified model uses these limits for the diurnal variation in $h(t)$.

Figure 7 shows the profiles diffusivity, $K(z, 00:00)$ and $K(z, 12:00)$ from such a model run, with the resulting concentration profiles: all other parameters as per the "standard run" in Table 2. At midnight, the $C(z, 00:00)$ is relatively constant with height for $z<h$, that is within the mixing zone. Above this region there is no mixing, and the profile exhibits a near exponential decay with height. This is the effect of "leaving behind" some of the tracer, as the diffusion reduces to zero at that level, and the tracer equation at these levels being governed solely by the loss term. The higher levels being "left behind" earlier, and have had longer to decay.

At midday, the mixed layer is deeper (as a prognostic), and filled throughout with tracer from the surface. The profile is similar to that for a constant boundary layer depth shown on the right of Fig. 3. Note that the gradient of the diffusivity at the surface is unchanged, and approximates to Eq. (4)

Figure 8 shows the time series of 4 m concentration, $C_4(t)$, that result from varying the mixing depth. The form of $h(t)$ as a sinusoid is shown in the lower right panel with the surface forcing term, $J(t)$, in the upper right; both $J(t)$ and $h(t)$ are symmetric about LAN, but $C_4(t)$, shows a slower rate of increase during the afternoon than the subsequent decay in early evening. The effect is indicated by fitting a first order and a second order harmonic function to $C_4(t)$ in a similar manner to analysis of the NO_x data above. The difference in the maxima of the two functions is 0.98 h.

The asymmetry seen in the model output is similar to that observed in the diurnally averaged time series of NO_x for cloud free days presented in Fig. 2, but the magnitude of the second harmonic is less in the model output than in the NO_x data: the latter has a more distinct ski-jump appearance, with positive curvature during the increasing phase of the curve. The difference between the maxima is remarkably similar; 0.98 h for the model compared to 1.05 h for the NO_x.

The effect of varying boundary layer depth by an order of magnitude may be only part of the story, but the point being stressed is that simple diffusion, a loss term and

[EGU](#)

boundary layer depth can account for most of the variability observed in an NO_x time series. The model is admittedly over-simplified, in that there is undoubtedly complex air chemistry of differing time scales involved, and the actual diffusivity profiles are unrealistic; nevertheless, the visualisation of the twin processes of non-linear diffusion and decay are an aid to a more intuitive understanding of vertical transfer in the boundary layer.

5 Conclusions

A simple boundary layer diffusion model incorporating a loss process is shown to generate trace gas profiles having a number of general characteristics. For the case where there is no transfer out of the top of the boundary layer, and a flux of tracer at the surface, concentration profiles tend to log-linear forms. Time series from the model agree well with field measurements, and differences may be explained by significant variation in the boundary layer depth, itself a result of convection. The generalisations from the model help provide an intuitive understanding of the evolution of trace gas species, the form of profiles resulting from surface fluxes, and how tracer measurements can be sensitive to the height of the sample inlet.

References

Ambach, W.: The influence of cloudiness on the net radiation balance of a snow surface with high albedo, J. Glaciol., 13, 73–84, 1974.

Davis, D. D., Eisele, F., Chen, G., et al.: An overview of ISCAT 2000, Atmos. Environ., 38(32), 5363–5373 2004.

Tracer diffusion

P. S. Anderson

EGU

Dibb, J. E. and Jaffrezo, J. L.: Air-snow exchange investigations at Summit, Greenland: An overview, J. Geophys. Res. 102, 26 795–26 807, 1997.

Jones, A. E., Anderson, P. S., Wolff E. W., Turner, J., Rankin, A. M., and Colwell, S. R.: A role for newly forming sea ice in springtime polar tropospheric ozone loss? Observational evidence from Halley station, Antarctica, J. Geophys. Res., 111, D08306, doi:10.1029/2005JD006566, 2006.

King, J. C. and Anderson, P. S.: Heat and Water Vapour fluxes and Scalar Roughness Lengths over an Antarctic Ice Shelf, Bound.-Layer Meteorol., 69, 101–121, 1994.

King, J. C., Argentini, S. A., and Anderson, P. S.: Contrasts between summer time surface energy balance and boundary layer structure at Dome C and Halley stations, Antarctica, J. Geophys. Res., 111, D02105, doi:10.1029/2005JD006130, 2006.

Mahrt, L.: Stratified Atmospheric Boundary Layers, Bound.-Layer Meteorol., 90, 375–396, 1998.

Warren, S. G.: Optical Properties of Snow, Rev. Geophys. Space Phys., 20, 67–89, 1982.

EGU

EGU

Table 1. Coefficients of the harmonic fitted curves shown in Fig. 2 and the loss term fitting the observed lag.

name	Sunny				Cloudy		
	value	Max w.r.t LAN	τ		value	Max w.r.t LAN	τ
a_0 (mean)	14.47				6.93		
a_s	−14.63	3.32	2.44		−5.31	2.52	1.80
a_c	−3.70				−2.62		
b_s	−2.25	4.37			−0.27	2.53	
b_c	−2.29				−0.19		

EGU

Table 2. Values of internal parameters used to test the sensitivity of the model. The results of these changes are summarised in Fig. 5.

Parameter	h/m	U/ms^{-1}	z_0/m
standard	50	1	5×10^{-5}
change h	200		
change U		5	
change z_0			500×10^{-5}

EGU
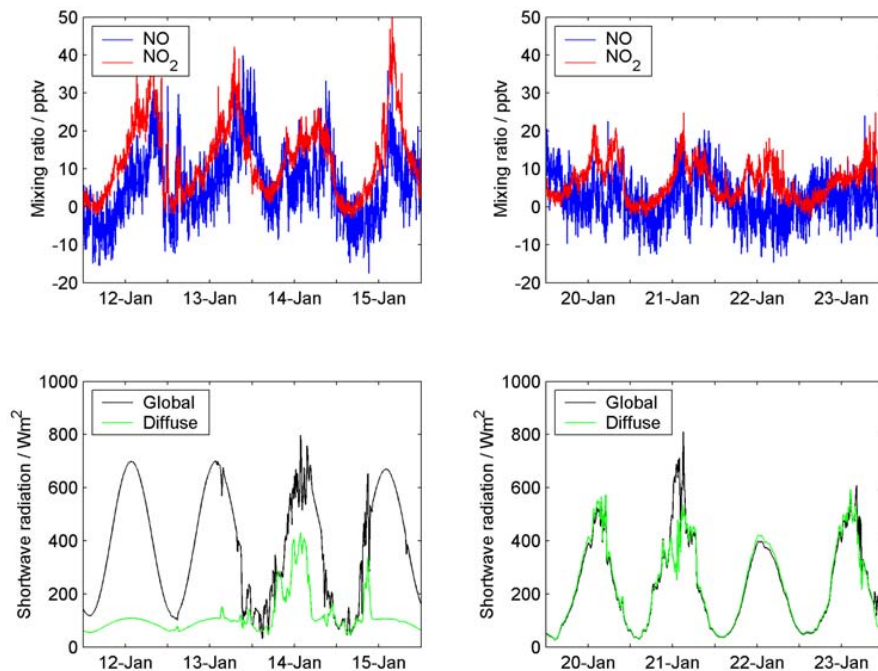
Fig. 1. Time series of NO and NO_2 during January 2005, compared to co-temporal data of solar radiation. The left hand panels are for days when there is little or no cloud cover, as indicated by the difference in the global and diffuse radiation series. The right hand panels are for cloudy days, when global and diffuse radiation are equal.
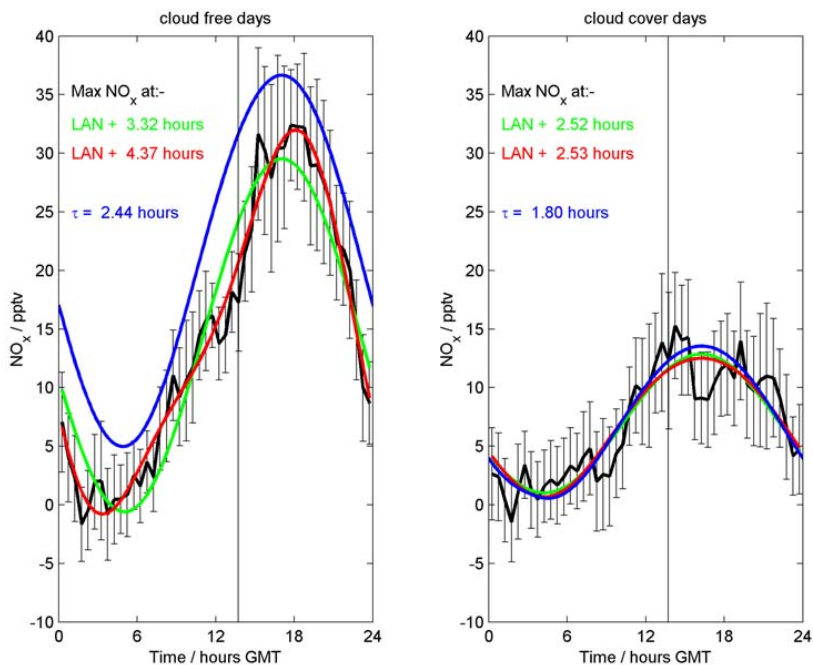
Fig. 2. Daily averaged time series of NO_x ($No + NO_2$) for the same data as in Fig. 1, with the cloud free data on the left and the cloud cover data on the right. Overlaid on each plot are three functions fitted to the binned data by least squares. In green and red are harmonic functions; the green function uses a single harmonic as per Eq. (6), the red function has first and second harmonics as per Eq. (7). For the cloud free days, the red curve is a significantly better fit, implying an asymmetry to the NO_x time series. The harmonic functions for the cloud cover data are equivalent. The blue curves show diffusion model fits, where τ has been tuned to give the same post-LAN maximum as the single harmonic function. For the cloud free data there is a significant mean discrepancy between the diffusion model and the data, whilst for the cloud cover days, this offset is absent, implying some real effect, and not an artefact of the instrument.

EGU

Tracer diffusion

P. S. Anderson

EGU
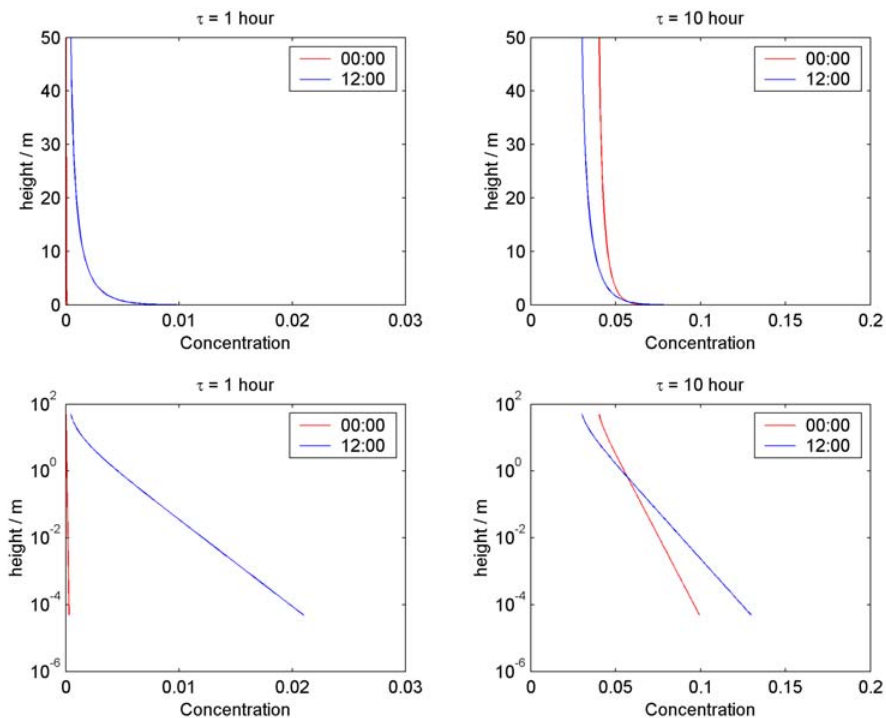
Fig. 3. Profiles of diffusion model concentration at midnight and midday for different values of loss term, τ. The profiles are plotted with both linear and log height axes. Note the change in scale for the concentration for the different values of τ. $J(t)$ forcing is for 15 November at 76° South.

EGU
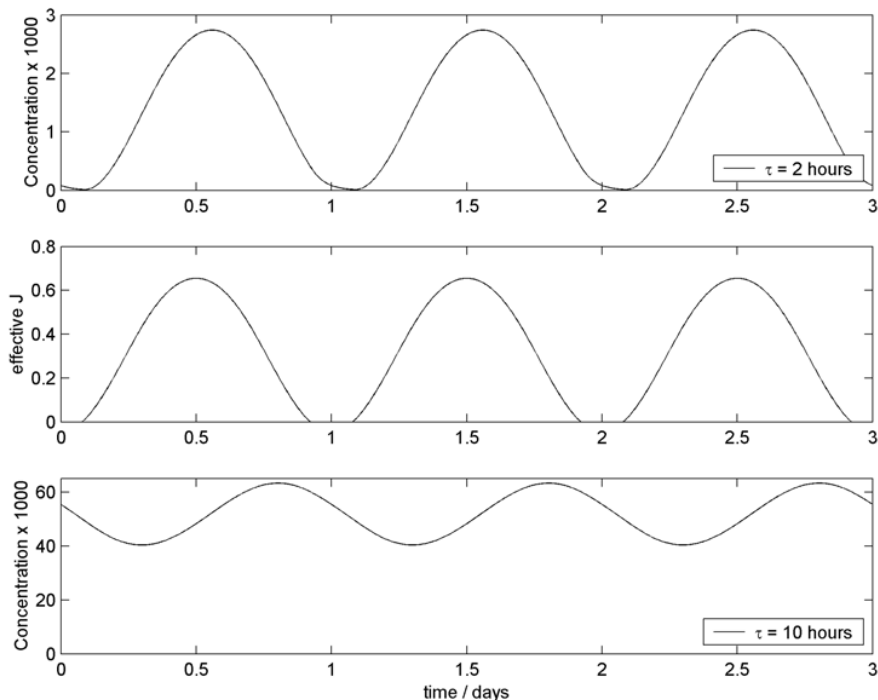
Fig. 4. Time series of diffusion model concentration at 4 m for the same model runs as Fig. 3. Three days of model output are shown, following five days of spin up; diurnal forcing is shown in the middle panel, and is identical for all model days, including spin up. The similarity of diurnal variation indicates that the model is in a periodic steady state.

EGU
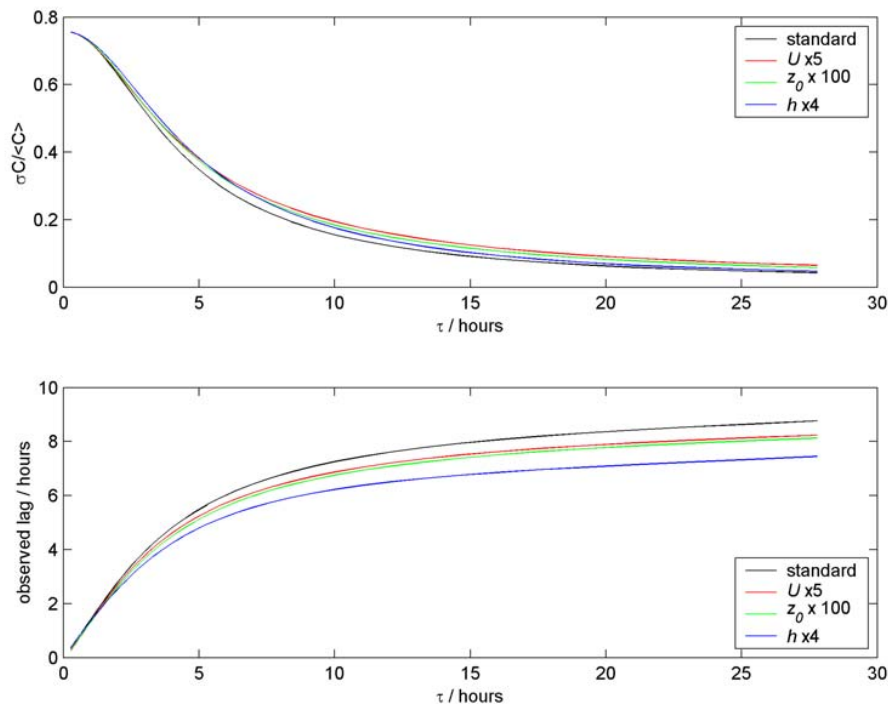
Fig. 5. Diffusion model normalised variance (upper panel) and lag relative to $J(t)$ (lower panel) as a function of loss term, τ. The relative insensitivity of the model to changes in other internal parameters (given in Table 2) is indicated by the four curves.

EGU
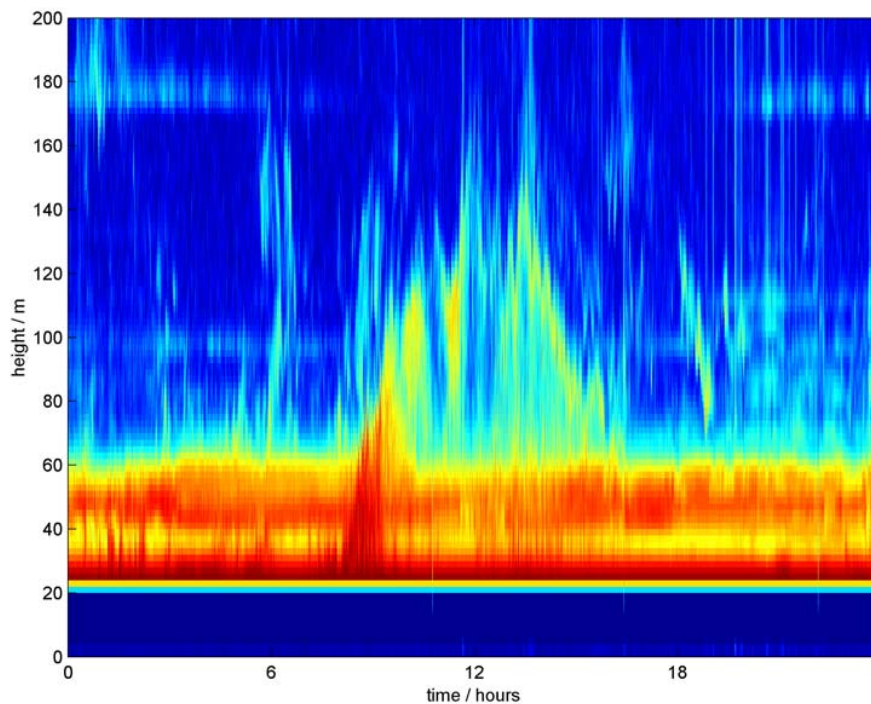
Fig. 6. Acoustic radar echogramme (sodar plot) for the 30 November, 2003, indicating the significant increase in mixing height around local apparent noon, starting at 07:00 and decaying by 17:00. Red/orange indicates strong echo from turbulence acting within a temperature gradient, end conversely, blue indicates minimal turbulent mixing. The lower levels are obscured by persistent echoes from nearby buildings.
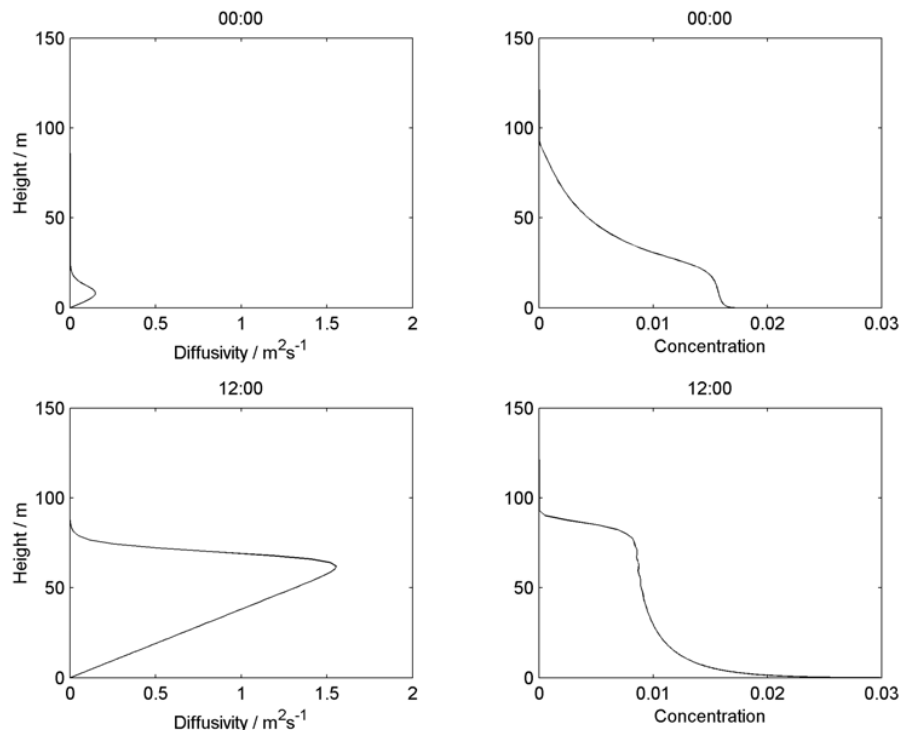
Fig. 7. Four metre tracer concentration profiles $C_4(t)$ for a time dependant diffusivity profile, $K(z, t)$. Upper panels are for midnight and lower panels for midday. The diffusivity profiles are shown on the left; near the surface $K(z, t)$ is proportional to height, with a smooth cut-off to zero at the proscribed mixing level height, $h(t)$. The resulting profiles of $C(z, t)$ are shown on the right, with a mixed layer underlying a decaying (non-diffusive) layer. $h(t)$ varies between the 00:00 minimum and the 12:00 maximum as a sinusoid.
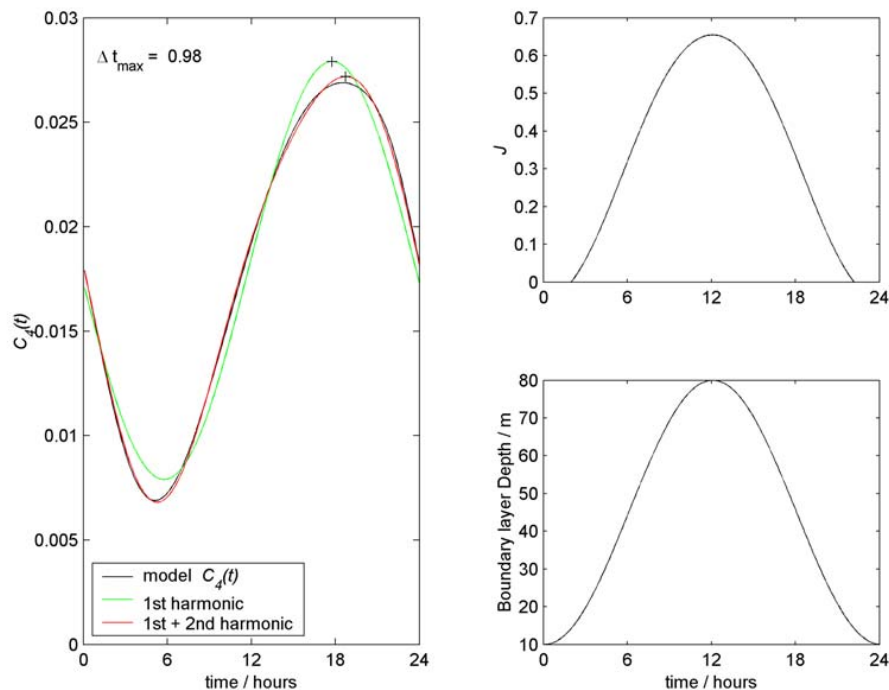
Fig. 8. Four metre tracer concentration time series, $C_4(t)$, for a model run where the effective mixing layer depth, $h(t)$, is time dependant. The proscribed surface flux is indicated by J, shown in the upper right panel; $h(t)$ is lower right . Both $J(t)$ and $h(t)$ are symmetric and centred on LAN. $C_4(t)$ is asymmetric as indicated by the fitted curves: a single harmonic (green) and 1st + 2nd harmonic (red). The maximum of each curve is shown, the time difference being 0.98 h.